Arab J Geosci (2017) 10: 437
DOI 10.1007/s12517-017-3227-2

ORIGINAL PAPER

A study into the behaviour of the formation level of an excavation under different unloading patterns in soft deposits

Yuqi Li[1] · **Xiaohui Chen**[1] · **Sam Divall**[2] · **Xiaodi Zhang**[1]

Received: 18 January 2017 / Accepted: 28 September 2017 / Published online: 9 October 2017

Abstract The construction of basements in urban areas is often associated with the possible damage to existing structures and services. The varying construction processes inevitably lead to different stress unloading patterns and therefore the dissipation of these excess pore-water pressures may lead to non-standard deformation profiles. The three main types of basement construction processes are layered excavation (LE), basin excavation (BE) and island excavation (IE). The effect of the various unloading patterns has been investigated by a three dimensional (3D) effective stress analysis method using the developed computer program 3DBCPE4.0. An excavation of length 50 m, width 50 m and depth 9 m in a certain homogenous and isotropic saturated soft soil was modelled. This included a diaphragm wall of 800-mm thickness embedded 18 m deep into the soft soil. The different excavation deformation profiles under different excavation patterns were related to the different unloading process, the exposure time of excavation face and the dissipation of negative excess pore-water pressures. The most favourable process for controlling the horizontal deformation of a retaining wall or the heave deformation of the formation level is suggested. The ground water potentials within the formation level are also presented.

Keywords Excavation pattern · Finite element method (FEM) · Negative excess pore-water pressure · Ground water potential

✉ Yuqi Li
liyuqi2000@shu.edu.cn

[1] Department of Civil Engineering, Shanghai University, Shanghai 200444, China

[2] Department of Civil Engineering, City University London, London EC1V 0HB, UK

Introduction

Excavation will cause the deformations of retaining structure, pit base and ground surface; therefore, numerous investigations on the characteristics of excavation-induced deformations have been performed. Ou and his research group did a lot of research; they proposed an empirical method for predicting the spandrel and concave settlement profiles on the basis of a regression analysis of the field observations of settlement curves (Hsieh and Ou 1998), studied building responses and ground movements caused by an excavation using the top-down construction method (Ou et al. 2000), analysed basal heave of excavations (Hsieh et al. 2008), evaluated basal heave stability (Do et al. 2013) and investigated extensively the behaviour of excavations with cross walls (Hsieh et al. 2012, 2013; Ou et al. 2013; Wu et al. 2013). In addition, Zdravkovic et al. (2005), Kung et al. (2007a, b) and Finno et al. (2007) studied the deformation behaviour of excavation in other aspects. Excavation will also cause the variation of pore pressure due to unloading. In order to investigate variation of pore-water pressure induced by excavation, 3D effective stress analysis based on Biot's consolidation theory was performed. Osaimi and Clough (1979) investigated pore-water pressure dissipation during an excavation based on Biot's consolidation theory. Benmebarek et al. (2006) analysed the effect of seepage flow on the lateral earth pressures acting on deep sheet piled wall excavations in cohesionless soil using the explicit finite difference method implemented in Fast Lagrangian Analysis of Continua (FLAC) code. The distribution rules of the formation level deformations and excess pore-water pressure were analysed in detail integrating the time parameter by Li et al. (2008). Borges and Guerra (2014) analysed the consolidation-dependent behaviour of a cylindrical excavation in a clayey soil. The study investigated the influence of the diameter of excavation, the embedded length of the wall and the elastic modulus of the wall material on the behaviour of the formation level. In actual engineering, there

are different excavation patterns according to the surrounding environment and the stability of excavation. Layered excavation (LE) is that soil is excavated uniformly from the excavation, basin excavation (BE) is that the soil at the formation level centre is excavated first whereas the soil around the formation level centre is excavated later and island excavation (IE) refers to that the soil around the formation level centre is excavated first whereas the soil at the formation level centre is excavated later. However, as reported above, little work has focused on the effect of the excavation patterns (such as IE and BE) on the formation level. Tan and Wang (2013a, b) studied the characteristics of a circular excavation and its peripheral according to a large-scale deep excavations by the island technique. The study compared bottom-up construction of the central cylindrical shaft first and top-down construction of the peripheral rectangular excavation in Shanghai's soft clay. However, they concentrated on formation level shape (central circular and peripheral rectangular) and the construction method (bottom-up construction and top-down construction) via the analysis of formation level deformations. In this study, to explore the effects of excavation patterns on the behaviour of the formation level, based on Biot's consolidation theory, a computer program *3DBCPE*4.0 was developed by 3D FEM. This was used to perform the coupled analysis of soil mass deformation and pore-water pressure dissipation. LE, BE and IE were modelled respectively and the results are reported in this paper.

Biot's 3D consolidation finite element equations

Biot's 3D consolidation finite element equations (Potts and Zdravkovic 1999; Xie and Zhou 2002) can be written in the following form:

$$[K]\{\Delta U\}^e = \{\Delta R\}^e \tag{1}$$

where $[K]$ is the element consolidation matrix (a symmetric matrix of 32 × 32 since a mesh of eight noded hexahedral isoparametric elements is used to discretize a pit geometry in this paper), $\{\Delta U\}^e$ is the increment column matrix of unknown terms of element node and $\{\Delta R\}^e$ is the increment

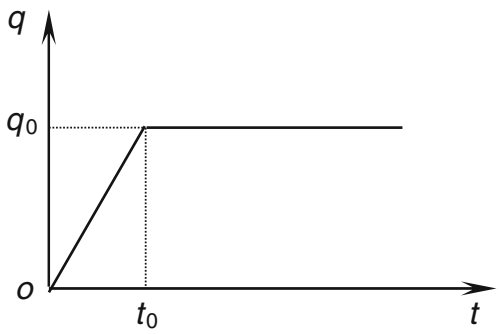

Fig. 1 Loading curve

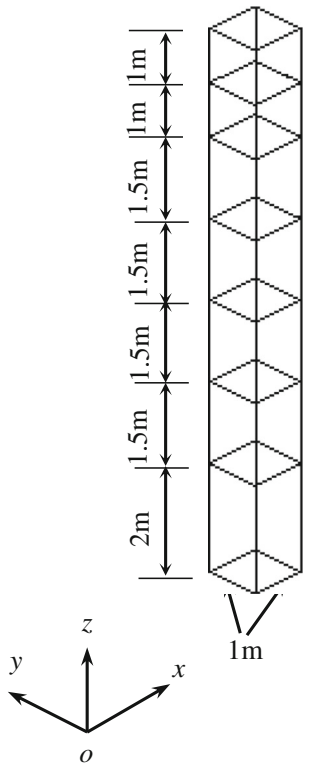

Fig. 2 Finite element mesh used for analysis of 1D consolidation

column matrix of equivalent load and water runoff of element node. The sub matrix of the $[K]$ matrix is given by:

$$[K_{ij}] = \begin{bmatrix} [K_{eij}] & [K_{cij}] \\ [K_{cji}] & -\theta\Delta t K_{sij} \end{bmatrix} \quad (i = 1, 2, \ldots, 8) \tag{2}$$

where θ is the integration constant which ranges from 0.5 to 1.0, $[K_{eij}]$ is the sub matrix of element stiffness matrix, $[K_{cij}]$ is the sub matrix of element coupling matrix and K_{sij} is the component of element seepage matrix (Xie and Zhou 2002). The sub matrices of the $\{\Delta U\}^e$ and $\{\Delta R\}^e$ matrices can be expressed respectively as the following:

$$\{\Delta U_i\} = [\Delta u_i \;\; \Delta v_i \;\; \Delta w_i \;\; \Delta p_i]^T \; (i = 1, 2, \ldots, 8) \tag{3}$$

$$\{\Delta R_i\} = [\Delta R_{xi} \;\; \Delta R_{yi} \;\; \Delta R_{zi} \;\; \Delta R_{pi}]^T \; (i = 1, 2, \ldots, 8) \tag{4}$$

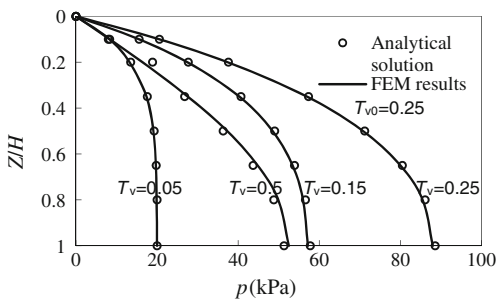

Fig. 3 Comparison of pore pressure

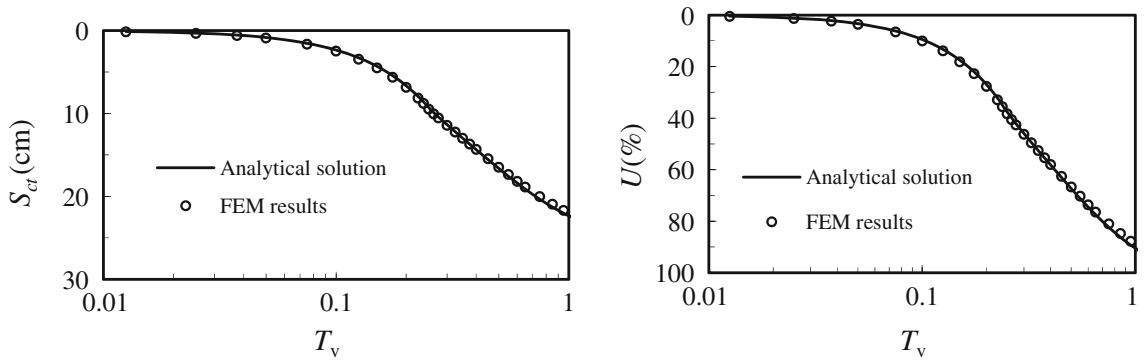

(a) settlement (b) average degree of consolidation

Fig. 4 Comparisons of settlement and average degree of consolidation

where Δu_i, Δv_i, Δw_i, and Δp_i are the displacement increments and the pore-water pressure increment of the ith element node, respectively, ΔR_{xi}, ΔR_{yi}, ΔR_{zi} and ΔR_{pi} are the equivalent load increments and the equivalent water runoff increment of the ith element node, respectively. The seepage effect induced by the water head difference between the inside and the outside of the formation level cannot be taken into account when analysing excavation deformation and pore-water pressure using Eq. (1). Thus, a ground water potential is introduced for consolidation analysis of the excavation. When neglecting the solute potential, the ground water potential of a saturated soil is defined by

$$P = p + \gamma_w z \tag{5}$$

where P is the ground water potential of a saturated soil, p is the sum of pressure potential (hydrostatic pressure) and load potential (excess pore-water pressure), i.e. the total pore-water pressure, the spatial coordinate z is upwards positive, γ_w is unit weight of water and γ_w z is the gravity potential. The ground water potentials of element node i at time t_n and t_{n+1} are represented by $P_{i(n)}$ and $P_{i(n+1)}$, respectively. Thus, Eqs. (3) and (4) may be written in the following form without regard to the influence of soil vertical displacement:

$$\{\Delta U_i\} = \left[\Delta u_i \quad \Delta v_i \quad \Delta w_i \quad P_{i(n+1)}\right]^T \quad (i = 1, 2, \ldots, 8) \tag{6}$$

$$\{\Delta R_i\} = \left[\Delta R'_{xi} \quad \Delta R'_{yi} \quad \Delta R'_{zi} \quad \Delta R'_{pi}\right]^T \quad (i = 1, 2, \ldots, 8) \tag{7}$$

where $\Delta R'_{xi} = \Delta R_{xi} + [K_{cij}]P_{i(n)}$, $\Delta R'_{yi} = \Delta R_{yi} + [K_{cij}]P_{i(n)}$, $\Delta R'_{zi} = \Delta R_{zi} + [K_{cij}]P_{i(n)}$ and $\Delta R'_{pi} = \Delta R_{pi} - \theta \Delta t K_{sij} P_{i(n)}$. Based on the finite element equations derived above, a 3D consolidation finite element program 3DBCPE4.0 was developed. In order to validate the program, an analysis of one-dimensional consolidation for homogeneous soft soils under time-dependent loading was introduced (Li et al. 2008). The soil layer top is pervious and free, and the bottom is impervious and fixed. Displacements perpendicular to the boundaries are restrained and an impermeable condition is assigned at the vertical boundaries. Soil parameters are Poisson's ratio $\mu = 0.301$, elasticity modulus $E = 3$ MPa, vertical permeability coefficient $k_v = 1.0 \times 10^{-8}$ m/s and thickness of soil layer $H = 10$ m. A load curve is shown in Fig. 1 where maximum load $q_0 = 100$ kPa and time $t_0 = 70$ days. Calculating domains in x-, y- and z-direction are 1, 1 and 10 m respectively and are divided into seven meshes, as shown in Fig. 2.

The comparisons of pore pressure, settlement and average degree of consolidation between the FEM results and the analytical solution of 1D consolidation are shown in Figs. 3 and 4. The results of FEM agree very well with those of the analytical solution, which proves the validity of the program, so it can be used for effective stress analysis.

Stress-strain relationship of soil

Soil behaviour was simulated using the revised Duncan-Chang model (Duncan and Chang 1970; Kulhawy and Duncan 1972) in this paper. The model assumes a hyperbolic stress-strain relationship and a variable Poisson's ratio by

Table 1 Soil parameters used during modelling

K	n	R_f	c' (kPa)	φ' (°)	F	G	D	K_{ur}	k_h (m/s)	k_v (m/s)	γ' (kN/m^3)
150	0.7	0.85	15	35	0.15	0.35	3.5	300	1.0×10^{-8}	1.0×10^{-8}	9

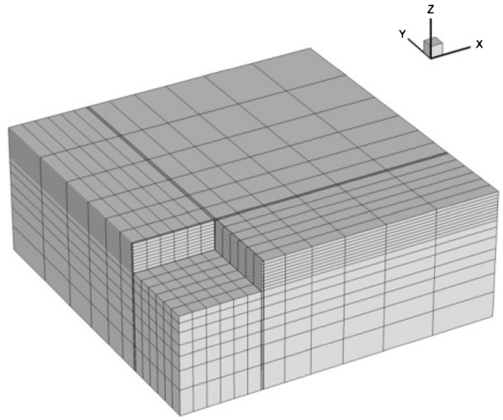

Fig. 5 Mesh of finite elements

means of stress-dependent Poisson's ratio (Kulhawy and Duncan 1972). The initial modulus is defined as

$$E_i = Kp_a\left(\frac{\sigma_3}{p_a}\right)^n \tag{8}$$

where the modulus number K and modulus exponent n are dimensionless material parameters; σ_3 is the minor principal stress; p_a is atmospheric pressure expressed in the same pressure units as σ_3. When the stress-strain relationship is employed in incremental form, the tangent modulus corresponding to any point on a stress-strain curve can be expressed as follows:

$$E_t = \left[1-\frac{R_f(1-sin\varphi)(\sigma_1-\sigma_3)}{2ccos\varphi+2\sigma_3 sin\varphi}\right]^2 Kp_a\left(\frac{\sigma_3}{p_a}\right)^n \tag{9}$$

where c and φ are Mohr-Coulomb strength parameters; σ_1 is the major principal stress; and R_f is the failure ratio. When $(\sigma_1-\sigma_3)$ is less than its historical maximum, it is assumed that the soil is under unloading or reloading and the tangent modulus is defined as

$$E_{ur} = K_{ur}p_a\left(\frac{\sigma_3}{p_a}\right)^n \tag{10}$$

where K_{ur} is the unloading-reloading modulus number and is always greater than the primary loading modulus number K. The initial Poisson's ratio can be expressed as

$$\nu_i = G-Flog\left(\frac{\sigma_3}{p_a}\right) \tag{11}$$

and the tangent Poisson's ratio

$$\nu_t = \frac{\nu_i}{\left(1-A^*\right)^2} \tag{12}$$

where $A^* = \frac{(\sigma_1-\sigma_3)D}{Kp_a\left(\frac{\sigma_3}{p_a}\right)^n\left[1-\frac{R_f(1-sin\varphi)(\sigma_1-\sigma_3)}{2ccos\varphi+2\sigma_3 sin\varphi}\right]}$; and D, F and G are material parameters.

Studies on the behaviour of foundation pit under different excavation patterns

Numerical example and finite element model

A formation level of length 50 m, width 50 m and depth 9 m in a certain homogenous and isotropic saturated soft soil is presented. The diaphragm wall of 800 mm thickness is embedded 18 m deep in soft soil. The groundwater tables inside and outside the excavation were assumed to locate on the excavated surface and the ground surface, respectively. Soil vertical and horizontal permeability coefficients (i.e. k_h and k_v) are both 1.0×10^{-8} m/s and the effective unit weight of soil γ' is 9.0 kN/m^3 (Table 1).

Two layer struts of reinforce concrete are respectively set at 3 and 6 m under the ground surface. Their cross-sectional dimensions at the first tier and the second tier were 600 by 600 mm and 600 by 700 mm, respectively. The horizontal spaces between the struts within the excavation at every tier were 8.3 m. Given that the influence scope of an excavation and the symmetry about the formation level centreline, the dimensions of the model in x-, y- and z-direction are 100 (length) by 100 (width) by 40 m (depth). Finite element meshes of soil mass and retaining wall are shown in Fig. 5

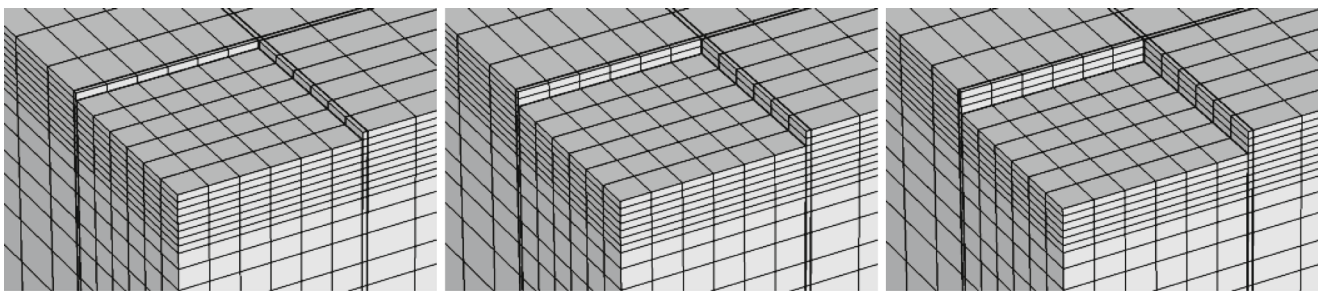

Fig. 6 Diagrams of LE process at stage 1

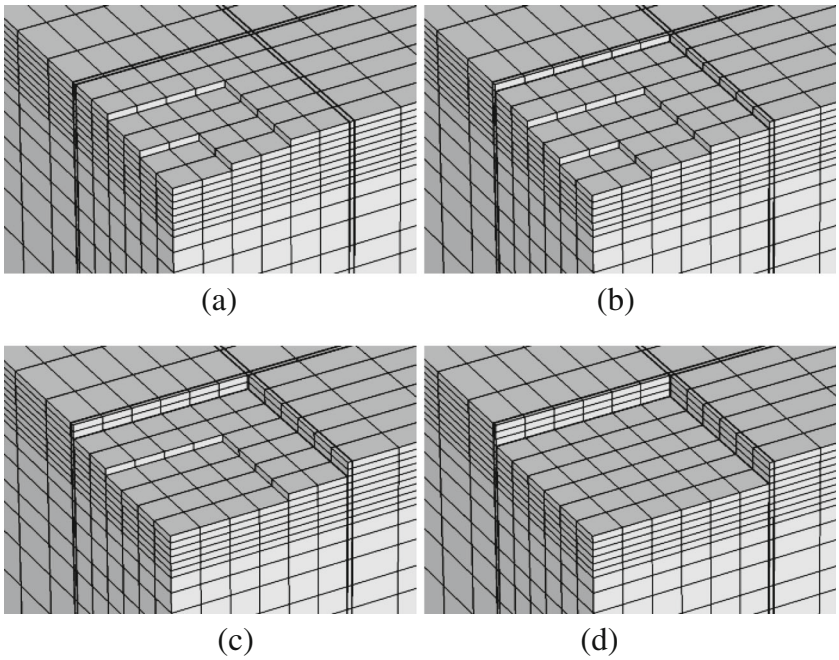

Fig. 7 Diagrams of BE process at stage 1

wherein the element size was fine near the walls where deformations and flow gradients are concentrated.

The bottom boundary of the excavation model was assumed to be fixed and displacements perpendicular to the boundaries were restrained at the lateral boundaries. As far as the hydraulic boundary conditions were concerned, a no-flow condition was assigned at the symmetrical plane and an impermeable condition was assigned at the vertical boundaries. The bottom boundary of the model was impermeable whereas the top was permeable and the retaining walls were double-sided impermeable. All soil units were discretized using eight-node hexahedral isoparametric elements and were simulated using the revised Duncan-Chang model. According to the studies of many researchers (Duncan and Chang 1970; Kulhawy and Duncan 1972; Ou et al. 1996; Liao 2009), the parameters of hyperbolic model in this paper are listed in Table 1. In Table 1, c' and φ' are the effective cohesion and the effective internal friction angle of soil, respectively. Retaining walls were modelled with a linear elastic model whose modulus of elasticity and Poisson's ratio are 25 GPa and 0.167, respectively. Retaining wall's elements were discretized using

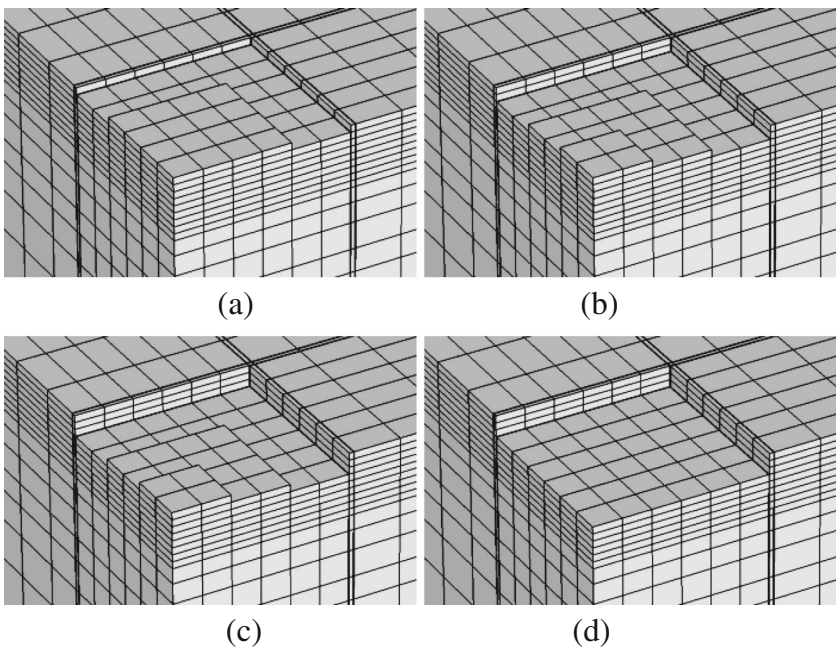

Fig. 8 Diagrams of IE process at stage 1

Table 2 LE process

Excavation stage	Process	Excavation thickness (m)	Total excavation depth (m)	Strut setting	Duration (day)
Stage 1	Excavation (a)	1.0	1.0	Nothing	1
	Excavation (b)	1.0	2.0	Nothing	1
	Excavation (c)	1.0	3.0	Nothing	2
	Intermission	0.0	3.0	Nothing	8
Stage 2	Excavation (a)	1.0	4.0	One layer	2
	Excavation (b)	1.0	5.0	One layer	2
	Excavation (c)	1.0	6.0	One layer	3
	Intermission	0.0	6.0	One layer	8
Stage 3	Excavation (a)	1.0	7.0	Two layer	3
	Excavation (b)	1.0	8.0	Two layer	3
	Excavation (c)	1.0	9.0	Two layer	4
	Intermission	0.0	9.0	Two layer	10

Excavation processes (a), (b) and (c) at the first stage are shown in Fig. 6

Wilson non-harmony elements. A row of 0.1-m-thick interfaces were used to connect soil mass and retaining wall elements. The two sides of the retaining wall adopted 3D thin interface elements which were derived from Yin's rigid plastic model (Yin et al. 1995) for outer friction angle=1.0° and cohesion=0.5 kPa (Wang 1994). Its other model parameters are the same as those of the soil mass elements. Supports were simulated with the linear elastic model with 23 GPa elasticity modulus and were discretized using spatial bar elements.

Construction process under different excavation patterns

LE, BE and IE all involved three stages and the excavated thickness at every stage was 3 m. Construction at every stage was divided into three or four stages to complete (see Figs.6, 7, 8). Excavation intermissions after every excavation stage were allowed for installation of struts or casting the formation level base concrete. Excavation duration each stage and the intermission duration after each stage under the different excavation patterns were also kept the same (as shown in Tables 2, 3, 4).

Deformation behaviour of excavation

Excavations will cause the horizontal displacement of retaining walls, ground surface settlements around the excavation and heave of the formation level. The excavation

Table 3 BE process

Excavation stage	Process	Maximum excavation depth (m)	Strut setting	Duration (day)
Stage 1	Excavation (a)	2.0	Nothing	1
	Excavation (b)	3.0	Nothing	1
	Excavation (c)	3.0	Nothing	1
	Excavation (d)	3.0	Nothing	1
	Intermission	3.0	Nothing	8
Stage 2	Excavation (a)	5.0	One layer	1
	Excavation (b)	6.0	One layer	2
	Excavation (c)	6.0	One layer	2
	Excavation (d)	6.0	One layer	2
	Intermission	6.0	One layer	8
Stage 3	Excavation (a)	8.0	Two layer	1
	Excavation (b)	9.0	Two layer	3
	Excavation (c)	9.0	Two layer	3
	Excavation (d)	9.0	Two layer	3
	Intermission	9.0	Two layer	10

Excavation processes (a), (b), (c) and (d) at the first stage are shown in Fig. 7

Table 4 IE process

Excavation stage	Process	Maximum excavation depth (m)	Strut setting	Duration (day)
Stage 1	Excavation (a)	2.0	Nothing	1
	Excavation (b)	3.0	Nothing	1
	Excavation (c)	3.0	Nothing	1
	Excavation (d)	3.0	Nothing	1
	Intermission	3.0	Nothing	8
Stage 2	Excavation (a)	5.0	One layer	1
	Excavation (b)	6.0	One layer	2
	Excavation (c)	6.0	One layer	2
	Excavation (d)	6.0	One layer	2
	Intermission	6.0	One layer	8
Stage 3	Excavation (a)	8.0	Two layer	1
	Excavation (b)	9.0	Two layer	3
	Excavation (c)	9.0	Two layer	3
	Excavation (d)	9.0	Two layer	3
	Intermission	9.0	Two layer	10

Excavation processes (a), (b), (c) and (d) at the first stage are shown in Fig. 8

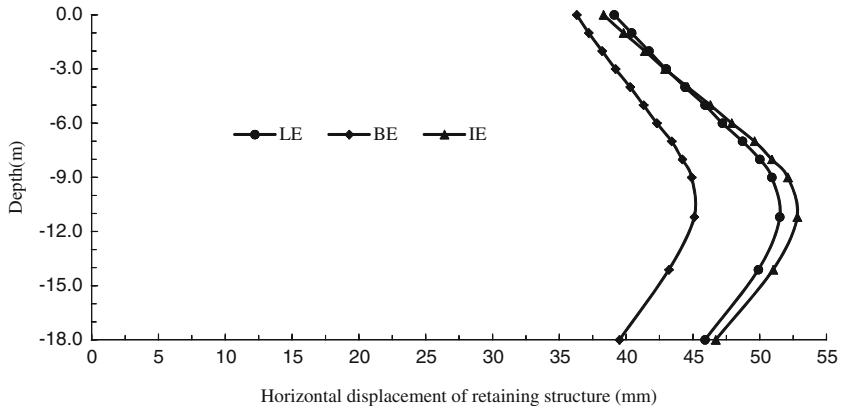

Fig. 9 Displacement of retaining structure at the third excavation stage

deformations under LE, BE and IE are analysed and investigated by the comparison of the following:

1. The horizontal displacement of retaining wall,
2. The ground settlement around foundation pit, and
3. The heave of pit base.

Figure 9 shows the horizontal displacement comparison at the $x = 0$ section and at the third (final) excavation stage. The maximum horizontal displacements under the different excavation patterns all occur at approximately 2 m under the excavation surface (i.e. 11 m under the surface level). In the case of BE, the maximum horizontal displacement decreases by 12.4% and under IE it increases by 2.5% compared with LE. The different horizontal displacements of the retaining wall under the excavation patterns were induced by changing the process of applying the earth pressure acting on the retaining structure within the excavation. Take the first excavation stage, for example, the exposure time of the retaining wall within the excavation at the end of the first excavation intermission is shown in Table 5. The horizontal displacement comparison at the $x = 0$ section and at the end of the first excavation intermission is indicated in Fig. 10. The retaining wall has a cantilever-type deflection because the excavation was carried out without a strut installation at the first stage. It can be seen from Table 5 and Fig. 10 that the lateral

Table 5 Exposure time of retaining wall

Depth range of retaining wall (m)	BE (day)	LE (day)	IE (day)
0 ~ 1	10	11	11
1 ~ 2	9	10	10
2 ~ 3	8	8	9

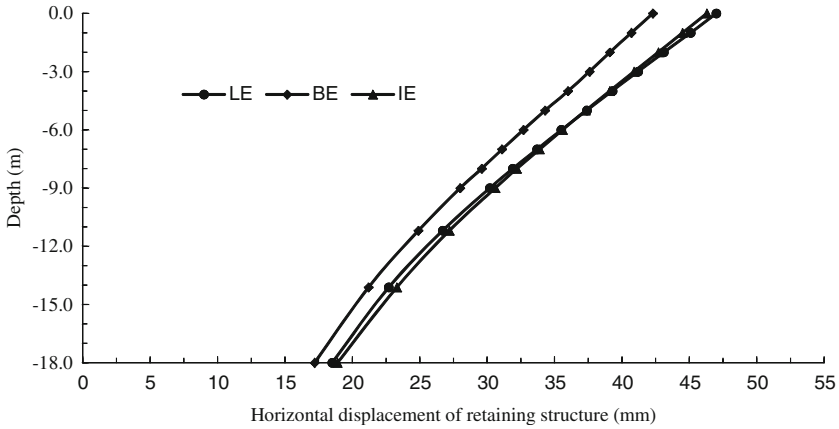

Fig. 10 Displacement of retaining structure at the end of the first excavation intermission

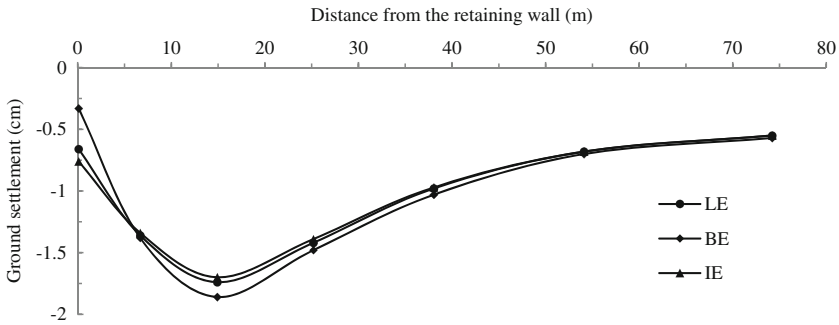

Fig. 11 Ground settlement at the third excavation stage

displacements of the retaining wall under BE are smaller than those under LE and IE. Since the exposure time of the retaining structure was the shortest under BE (0–2 m depth range), the duration that the lateral earth pressure acting on the retaining wall inside the excavation was zero was the shortest. The moment acting on retaining wall was induced by the lateral earth pressure outside the excavation at 0–2 m depth range which is larger than the one at 2–3 m depth range. The duration that the lateral earth pressure acting on the 2–3 m depth range of retaining wall inside the excavation under IE was zero was slightly larger than under LE leading to the lateral displacements of the retaining wall under IE and LE being very close. Therefore, the soil around the retaining structure inside the excavation under BE was excavated later and the exposure time of the retaining wall decreased. This was more favourable for controlling the deformation of retaining wall.

Figure 11 shows the ground surface settlement around the formation level at the $x = 0$ section under the three different excavation patterns after the third excavation stage. It can be seen from Fig. 11 that the maximum settlement occurred at 15 m from the formation level and the settlement profiles were concave (similar to Hsieh and Ou 1998). The excavation patterns have little influence on the ground surface settlement. Within 6 m from the formation level, the settlement values, under BE, were smaller than those of LE. IE had larger settlements because the wall deflection effects the soil near the formation level. The wall displacements under BE were

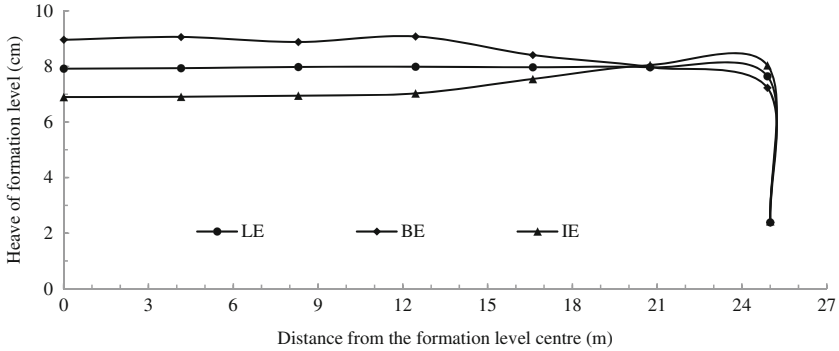

Fig. 12 Heave of formation level at the third excavation stage

Table 6 Exposure time of excavation face at the end of the first excavation intermission

Distance from centre (m)	LE (day)	BE (day)	IE (day)
0–8.3	8	10	8
8.3–16.6	8	9	9
16.6–25	8	8	10

similar and the negative excess pore-water pressures under BE were slightly larger according beneath the retaining wall.

The comparison of formation level basal heave at the $x = 0$ section and under three different excavation patterns at the third excavation stage is shown in Fig. 12. It can be seen from Fig. 12 that within 21 m from the centre of the formation level, the heave values of the base under BE were the largest. The equivalent values resulting from LE were larger or almost equal and the values under IE were the smallest. However, within 21–25 m from the formation level centre, the heave values under

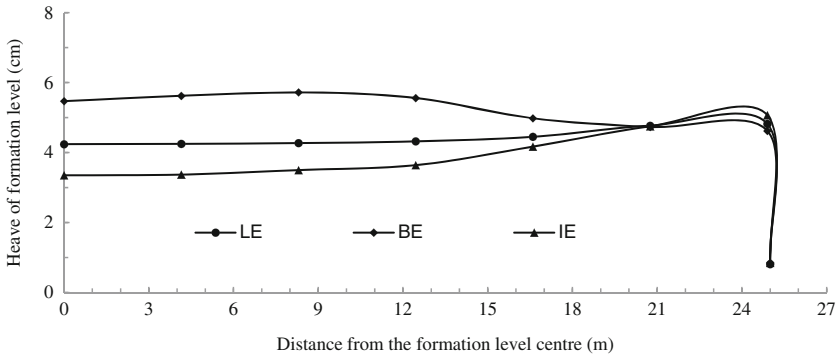

Fig. 13 Heave of formation level at the end of the first excavation intermission

smaller than the ones under LE and IE (Figs. 9 and 10) and so the lateral pressures of the soil outside the excavation under BE were larger. The vertical stress of the soil outside the excavation under the three construction patterns were approximately the same, i.e. the smaller horizontal displacement means the larger confining pressure of the soil outside the excavation. This will inhibit the settlement of the soil outside the excavation thus the ground settlements under BE were smaller than those from LE and IE. Beyond 6 m away from the formation level, the settlement values under BE were the largest. Settlement values under LE and IE were smaller or approximate the same. This was because the ground settlements far from the formation level were mainly influenced by the change of the effective stress from the change in excess pore-water pressure (Figs.17, 18, 19). The distributions of excess pore-water pressure outside the excavation were different excavation patterns were very approximate and they all decreased sharply close to the retaining wall due to the friction between soil and retaining wall. For LE, the soil was excavated uniformly from the excavation and the self-gravity stress was therefore released uniformly. This leads to the uniform heave of formation level base. For BE, the soil at the formation level centre was excavated first, whereas the soil around the formation level centre was excavated later, so larger heave values occur at the centre. The process of IE is opposite to BE and smaller heave occurs at the centre. Compared with the maximum heave value of the formation level base under LE (within 15 m from the pit centre), the BE value increases by 13.6% and under IE the value decreases by 12%. Therefore, as far as the heave stability of the formation level is concerned IE is more favourable and BE is least favourable. To further analyse the differences of formation level heave from the different

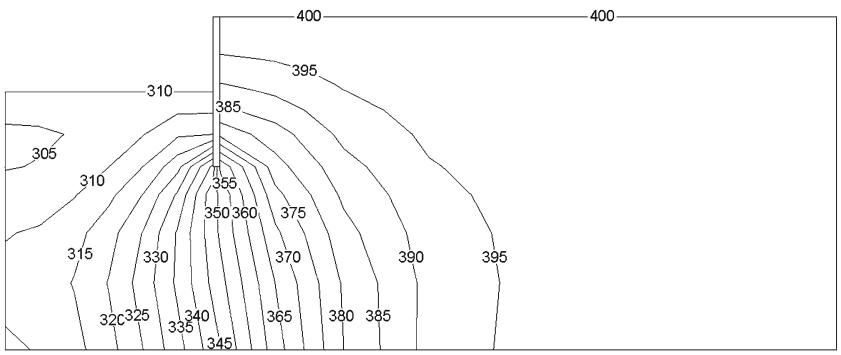

Fig. 14 Distribution of the soil water potentials under LE (unit: kPa)

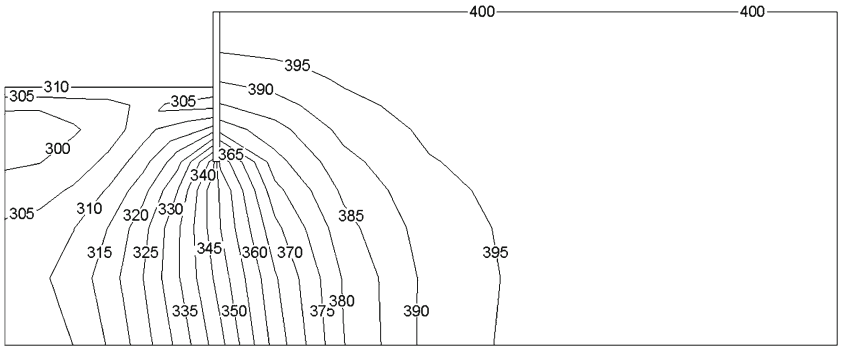

Fig. 15 Distribution of the soil water potentials under BE (unit: kPa)

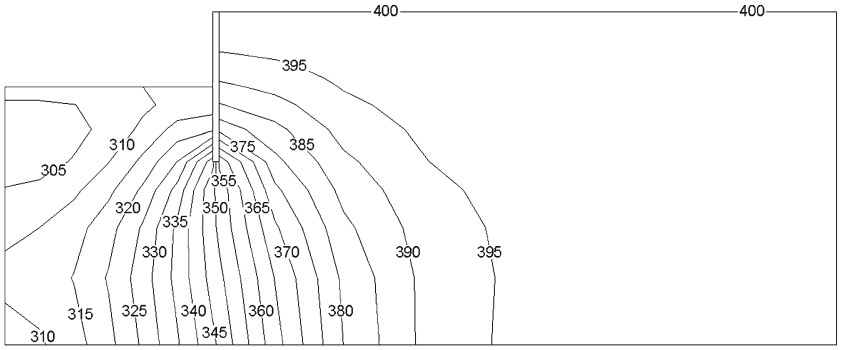

Fig. 16 Distribution of the soil water potentials under IE (unit: kPa)

excavation patterns, the heave and the exposure time of excavation face at the end of the first excavation intermission were examined (see Table 6 and Fig. 13). The unloading of the soil mass decreases the total stress of the soil beneath the excavation face and induces negative excess pore-water pressures. The longer the exposure time of excavation face was, the more the negative excess pore-water pressure dissipated; therefore, the decrease in effective stress beneath the excavation face was greater and the heave of pit base was larger. It can be seen from Table 6 and Fig. 13 that (within 8.3 m from the formation level centre) the exposure time under BE was the longest and therefore the heave of the base was the largest. During IE, the thick soil layer in the formation level centre was excavated later (as mentioned above) and the negative excess pore-water pressures dissipated slowly. Therefore, the heave deformations under IE were smaller than those under LE and BE.

Pore-water pressure of excavation

The flow of ground water depends on soil water potential and defined as the sum of excess pore-water pressure, hydrostatic pressure and the gravity potential. In order to analyse the flow of ground water inside and outside the excavation, under different excavation patterns, the contours of the soil water potentials inside and outside the excavation at the $x = 0$ section and at the third excavation stage are shown in Figs.14, 15, 16, where the datum for the elevation head is at the bottom boundary of model. It can be seen from Figs.14, 15, 16 that the soil

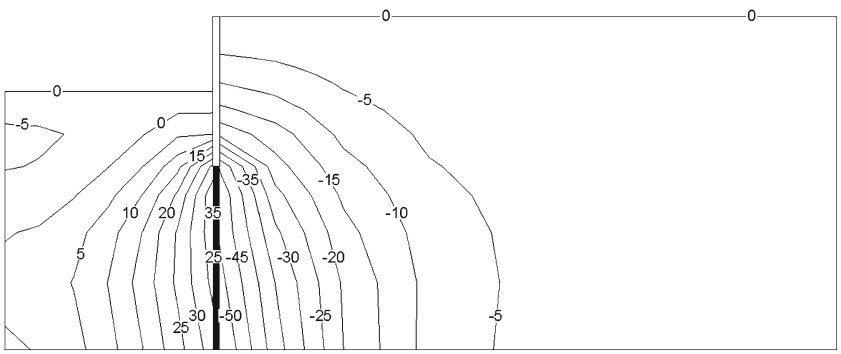

Fig. 17 Distribution of excess pore-water pressures under LE (unit: kPa)

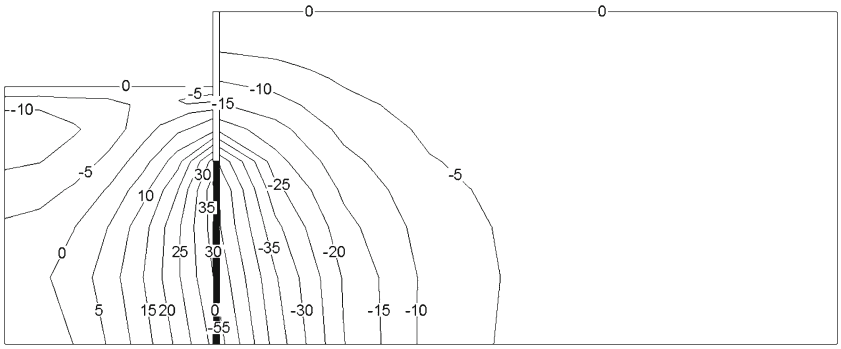

Fig. 18 Distribution of excess pore-water pressures under BE (unit: kPa)

water potentials outside the excavation were all larger than the ones inside under the three excavation patterns at the third excavation stage. Therefore, ground water flows into the excavation from the outside. For BE, ground water not only flows into the centre under excavation face but also observably flows into the area near to the retaining structure. Since the soil close to the retaining wall was unloaded later and the soil water potentials were also correspondingly less than the values under LE. Similarly, the soil at the formation level centre under IE was excavated later and the dissipation of the soil water potential at the centre was slow. Therefore, the ground water was more apt at flowing into the excavation at the formation level centre than during LE.

Figures 17, 18, 19 show the contours of the excess pore-water pressures inside and outside the excavation under the three patterns at the $x = 0$ section and at the third excavation stage. It can be seen from Figs. 17, 18, 19 that at the third excavation stage, the horizontal distribution range of the negative excess pore-water pressures beneath excavation face under LE were the smallest. The values under BE were the largest and the values under IE were between these two. However, the vertical distribution range of the negative excess pore-water pressures beneath excavation face under IE was the largest and the value under LE was the least. The comparison among the values of negative excess pore-water pressure under different excavation patterns shows that the dissipation of negative excess pore-water pressure under IE was the slowest.

The distribution difference of excess pore-water pressure is related to the unloading process of the three excavation patterns. The unloading process of LE was uniform and the exposure time of the whole excavation face was kept the same. This was favourable to the uniform dissipation of excess pore-water pressure and so its scope was small. During the process of BE and IE, the unloading above the excavation face was non-uniform. The unloading under BE was from the formation level centre to the retaining wall and it was just contrary under IE which is unfavourable for the dissipation of the excess pore-water pressures. The negative excess pore-water pressures under BE and IE dissipated slower and their areas were larger. In the process of BE, larger negative excess pore-water pressures were generated in the nearby retaining structure than the values under LE as the result of the later unloading nearby retaining structure under BE. Moreover, the process of IE was contrary to the one of BE and so its negative excess pore-water pressures at the formation level centre were larger than the LE values.

Conclusions

3D effective stress analysis of an excavation under layered, basin and island excavation processes was performed and reported in this work. This has led to the following conclusions: (1) the soil around retaining wall was unloaded later under BE which decreased the exposure time of the retaining structure and induced small horizontal displacements. It is, therefore, favourable when controlling the deformation of a retaining wall. The soil at the formation level centre was unloaded later

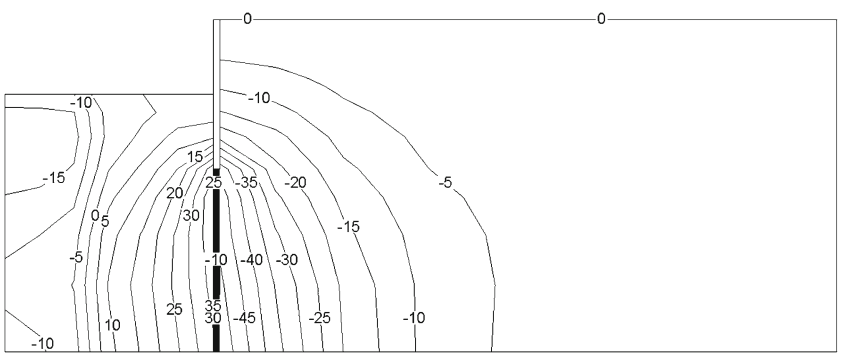

Fig. 19 Distribution of excess pore-water pressures under IE (unit: kPa)

under IE which decreased the exposure time of excavation face and caused small heave of base and can be considered favourable when controlling any heave deformation of the formation level. (2) The settlement of the soil near the retaining wall was related to the wall deflection; however, the settlement of soil at a reasonable distance from the wall was related to the dissipation of negative excess pore-water pressure. For example, the greater the negative excess pore-water pressure was then the greater the effective stress of soil was and resulting in larger soil settlement. (3) The distributions of total soil water potential and negative excess pore-water pressure were both very similar under the three excavation patterns. Since the order of unloading inside the excavation was different, then the scope of the negative excess pore-water pressure was larger (at the excavation face) for the soil which was unloaded last. In this work, only the excavation patterns were focused on; however, excavation is an over-consolidation problem due to unloading. Therefore, over-consolidation problem should be considered when choosing a constitutive model of soil in future investigations.

References

Benmebarek N, Benmebarek S, Kastner R, Soubra AH (2006) Passive and active earth pressures in the presence of groundwater flow. Geotechnique 56(3):149–158

Borges JL, Guerra GT (2014) Cylindrical excavations in clayey soils retained by jet grout walls: numerical analysis and parametric study considering the influence of consolidation. Comput Geotech 55:42–56

Do TN, Ou CY, Lim A (2013) Evaluation of factors of safety against basal heave for deep excavations in soft clay using the finite-element method. J Geotech Geoenviron 139(12):2125–2135

Duncan JM, Chang CY (1970) Nonlinear analysis of stress and strain in soils. J Soil Mech Found Div ASCE 96(SM5):1629–1653

Finno RJ, Blackburn JT, Roboski JF (2007) Three-dimensional effects for supported excavations in clay. J Geotech Geoenviron 133(1):30–36

Hsieh PG, Ou CY (1998) Shape of ground surface settlement profiles caused by excavation. Can Geotech J 35:1004–1017

Hsieh PG, Ou CY, Liu HT (2008) Basal heave analysis of excavations with consideration of anisotropic undrained strength of clay. Can Geotech J 45:788–799

Hsieh PG, Ou CY, Shih C (2012) A simplified plane strain analysis of lateral wall deflection for excavations with cross walls. Can Geotech J 49:1134–1146

Hsieh PG, Ou CY, Lin YL (2013) Three-dimensional numerical analysis of deep excavations with cross walls. Acta Geotech 8:33–48

Kulhawy FH, Duncan JM (1972) Stresses and movements in Oroville Dam. J Soil Mech Found Div ASCE 98(SM7):653–655

Kung GTC, Hsiao ECL, Juang CH (2007a) Evaluation of a simplified small-strain soil model for analysis of excavation-induced movements. Can Geotech J 44:726–736

Kung GTC, Juang CH, Hsiao ECL, Hashash YMA (2007b) Simplified model for wall deflection and ground-surface settlement caused by braced excavation in clays. J Geotech Geoenviron 133(6):731–747

Li YQ, Zhou J, Xie KH (2008) Environmental effects induced by excavation. J Zhejiang Univ Sci A 9(1):50–57

Liao HJ (2009) Numerical analysis in geotechnical engineering (2nd edn). China Machine Press, Beijing (in Chinese)

Osaimi AE, Clough GW (1979) Pore-pressure dissipation during excavation. J Geotech Eng ASCE 105(4):481–498

Ou CY, Wu TS, Hsieh HS (1996) Analysis of deep excavation with column type of ground improvement in soft clay. J Geotech Eng ASCE 122(9):709–716

Ou CY, Liao JT, Cheng WL (2000) Building response and ground movements induced by a deep excavation. Geotechnique 50(3):209–220

Ou CY, Hsieh PG, Lin YL (2013) A parametric study of wall deflections in deep excavations with the installation of cross walls. Comput Geotech 50:55–65

Potts DM, Zdravkovic L (1999) Finite element analysis in geotechnical engineering: Theory. Thomas Telford Limited, London

Tan Y, Wang D (2013a) Characteristics of a large-scale deep foundation pit excavated by the central-island technique in Shanghai soft clay. I: Bottom-up construction of the central cylindrical shaft. J Geotech Geoenviron 139(11):1875–1893

Tan Y, Wang D (2013b) Characteristics of a large-scale deep foundation pit excavated by the central-island technique in Shanghai soft clay. II: Top-down construction of the peripheral rectangular pit. J Geotech Geoenviron 139(11):1894–1910

Wang GG (1994) Theoretical study on large strain of deep excavation. Ph.D Thesis, Tongji University, Shanghai (in Chinese)

Wu SH, Ching JY, Ou CY (2013) Predicting wall displacements for excavations with cross walls in soft clay. J Geotech Geoenviron 139(6):914–927

Xie KH, Zhou J (2002) Theory and application of finite element analysis in geotechnical engineering. Science Press, Beijing (in Chinese)

Yin ZZ, Zhu H, Xu GH (1995) A study of deformation in the interface between soil and concrete. Comput Geotech 17(1):75–92

Zdravkovic L, Potts DM, St John HD (2005) Modelling of a 3D excavation in finite element analysis. Geotechnique 55(7):497–513